

# Response Analysis and Comparison of a Spar-Type Floating Offshore Wind Turbine and an Onshore Wind Turbine under Blade Pitch Controller Faults

**Etemaddar, M.; Blanke, Mogens; Gao, Z.; Moan, T.**

*Published in:*
Wind Energy

*Link to article, DOI:*
10.1002/we.1819

*Publication date:*
2016

*Document Version*
Early version, also known as pre-print

# Response Analysis and Comparison of a Spar-type Offshore Floating Wind Turbine and an Onshore Wind Turbine under Blade Pitch Controller Faults

M. Etemaddar [a,b], M. Blanke [b,c], Z. Gao [a,b], T. Moan [a,b]
a. Department of Marine Technology, Norwegian University of Science and Technology (NTNU)
b. Center of Ship and Ocean Structures (CeSOS) , Norwegian University of Science and Technology (NTNU)
c. Automation and Control Group, Department of Electrical Engineering, Technical University of Denmark (DTU)

**Abstract**
This paper analyses the effects of three pitch controller faults on the responses of an onshore wind turbine and a spar-type offshore floating wind turbine. These faults include: a stuck blade pitch actuator, a fixed value fault and a bias fault of the blade pitch sensor. The faults are modeled in the controller dynamic link library and a short-term extreme response analysis is performed using the HAWC2 simulation tool. The main objectives of this paper are to investigate how different faults affect the performance of wind turbines for condition monitoring purposes and which differences exist in the structural responses between onshore and offshore floating wind turbines. Statistical analysis of the selected response parameters are conducted using the six 1-hour stochastic samples for each load case. For condition monitoring purpose, the effects of faults on the responses at different wind speeds and fault amplitudes are investigated by comparing the same response under normal operation. The severities of the individual faults are categorized by the extreme values of structural loads and the structural components are sorted based on the magnitude of the fault effects on the extreme values. The pitch sensor fixed value fault is determined as the most severe fault case and the shaft appears as the structural component that experiences the highest risk. The effects of fault conditions on the offshore floating and the onshore wind turbines are compared to investigate the potential differences. The results show that faults cause more damage to the tower and the yaw bearing for the onshore wind turbine and more damage to the shaft for the offshore floating wind turbine.

**Keywords**
Spar, Floating Wind Turbine, Onshore Wind Turbine , Offshore, OC3-Hywind, Pitch Actuator Fault, Pitch Sensor Fault, Pitch Controller Fault, Response Characteristics, Extreme Response

**Abbreviations**

| | | | |
|---|---|---|---|
| $OWT$ | Onshore Wind Turbine | SD | Standard Deviation |
| $FWT$ | Floating Wind Turbine | BEM | Blade Element Momentum method |
| $PASF$ | Pitch Actuator Stuck Fault | DLL | Dynamic Link Library |
| $PSBF$ | Pitch Sensor Bias Fault | BR | Blade Root |
| PSFV | Pitch Sensor Fixed Value fault | TB | Tower Bottom |
| $TTF$ | Time To Fault | YB | Yaw Bearing |
| RD | Relative Difference | SB | Shaft Bearing |
| OC3 | Offshore Code Comparison Collaboration | WS | Wind Speed |

**Nomenclature**

| | | | |
|---|---|---|---|
| $T_p$ | Spectral peak period [sec] | $\Omega_m$ | Measured rotor speed by shaft speed sensor [rpm] |
| $H_s$ | Significant wave height [m] | $\Omega_f$ | Filtered shaft speed measurement [rpm] |
| $U_m$ | 1-hour mean wind speed at an elevation of 10 m [m/s] | $\Omega_{ref}$ | Controller reference shaft speed [rpm] |
| $\lambda$ | Rotor tip speed ratio [-] | $\Omega_{dif}$ | Sensor and controller reference shaft speed difference [rpm] |
| $\beta$ | Blade pitch angle [deg] | $T_t$ | Fault development period [sec] |
| $\beta_{act}$ | Actuator pitch angle [deg] | $\tau_{ref}$ | Controller reference generator torque [Nm] |
| $\beta_m$ | Measured blade pitch angle by sensor [deg] | $KP$ | Proportional gain of the controller |
| $\beta_{mf}$ | Measured blade pitch angle by sensor under fault [deg] | $KI$ | Integral gain of the controller |
| $\beta_{dif}$ | Sensor and controller reference pitch angle difference [deg] | $KG$ | Gain scheduling function |
| $\beta_{F0}$ | Fault amplitude [deg] | $KK$ | Gain scheduling constant |
| $\beta_{ref}$ | Controller reference pitch angle [deg] | $t$ | Time variable [sec] |

## 1. Introduction

In modern wind turbines, the controller system faces a multi-objective task. The controller was designed primarily to increase the efficiency of wind turbines by adjusting the slip ratio of the generator and to convert fixed-speed wind turbines to variable-speed wind turbines. Moreover, an additional controller was used to adjust the pitch angle of the wind turbine blade for wind speeds larger than the rated one to reduce the aerodynamic loads on the rotor while keeping constant power absorption. For offshore floating wind turbines (FWT), the controller can be used to improve the dynamic responses of the system and reduce the responses of the floating substructure [1].

Regardless of the type of wind turbine, the controller system consists of three main sub-systems: sensors, actuators and logical algorithms. Sensors are used to measure certain time varying parameters of the system and inputs to the controller algorithm, i.e., the generator shaft speed and blade pitch angle. The actuators are used to change the rotor blade pitch angle and generator torque. The controller algorithm provides time-dependent reference values to the actuators based on instantaneous variations in the sensor measurements to achieve selected predefined target responses. The controller objectives

can only be satisfied with sound operation of all three sub-systems. Faults or malfunctions of any sub-system can reduce the efficiency of the wind turbines and increase the structural loads, which consequently reduce the expected life-time of the wind turbines as well as operational safety.

In recent years, the effect of faults in different wind turbine components on the loads and responses of the wind turbines has been studied. For example, several wind turbine fault cases were simulated in the CONMOW [2] project, including: rotor mass and aerodynamic imbalances and blade pitch bearing friction. The aim was to study the resulting output and identify the most reliable signal for condition monitoring. The steady-state response of a parked spar-type offshore floating wind turbine as a function of blade pitch mechanism faults was studied by Jiang et al. [3] and results showed that a fault with one seized blade often leads to the largest platform roll and yaw angles. The effects of faults on the loads and power output of onshore wind turbines have been studied [4-6] for fault detection and isolation as well as structural load analysis purposes. Diagnoses and fault-tolerant control methodologies were applied in offshore engineering area by Fang et al. (2013) [7] in which the safety of structural elements was of high concern. Faults in the blade root bending moment strain gauges were simulated for a wind turbine with an individual pitch controller [8]. Active diagnosis was employed by Brath et al. (2011) [9] to isolate the bending moment and pitch sensor faults. Sensor and actuator fault detection for wind turbine systems was studied by Wei and Verhaegen [10] and different types of faults in the generator and rotor speed sensors were modeled and detected by Odgaard and Stoustrup [5, 6]. Different techniques for fault detection based on SCADA data analysis were described to identify incipient faults in wind turbines[11] and the pitch system data were used to monitor the health of the blade pitch system [12]. Generic techniques based on wavelet analysis were shown by Yang et al. (2010)[13] to have the potential to capture multiple types of faults in both mechanical and electrical elements of the wind turbines.

Despite its importance for the deployment of floating offshore wind turbines, notably little research has been conducted on the effects of particular faults on wind turbine components and therefore on reliability. This study aims to provide quantitative and qualitative information on the effects of different pitch actuator and controller faults on the loads and structural responses of a floating offshore wind turbine. The OC3 (Offshore Code Comparison Collaboration)-Hywind wind turbine [14], a 5-MW variable-speed pitch-regulated offshore floating wind turbine (FWT) with a spar-type sub-structure and catenary mooring lines, is used as the reference offshore floating wind turbine and an NREL 5-MW land-based wind turbine is used as the reference onshore wind turbine (OWT) in this study. The HAWC2 [1, 15] code, an aero-hydro-servo-elastic code for time-domain simulation of offshore wind turbines, is used to simulate the responses of the wind turbines under different operational conditions. The code is benchmarked via IEA code-to-code comparisons [16].

The objectives of this work are two-fold: 1) to describe the relationship between the given faults (pitch controller system faults) and the change in the responses of the wind turbine for condition monitoring purposes and 2) to perform a structural load analysis under fault conditions, including an extreme value analysis for structural design purposes. To this end, three fault cases in the blade pitch controller are modeled and simulated. These fault cases include two pitch sensor encoder faults i.e., a pitch sensor fixed value (PSFV) and a pitch sensor bias fault (PSBF), and one pitch actuator fault, i.e., a pitch actuator stuck fault (PASF). An indication of such fault could be caused by a real fault in the pitch system or by a fault in the sensor that measures pitch angle. Consistency check between the different blade pitch angles could be used for fault detection but this would not isolate the root cause of the fault. This paper does not address the fault diagnosis as such since there is already is a rich literature on wind turbine fault diagnosis. This paper is meant to contribute by analyzing the effects that faults have on structural responses and how they affect the ultimate safety of a wind turbine. This means that when fault diagnosis/prognosis indicates a certain fault, our results show which faults could be acceptable for limited time continued operation of a turbine until a repair could be made and which faults would need to be accommodated by fault-tolerant methods [17] if continued operation should be allowed. To investigate a measurable response characteristic for fault detection, the responses under fault conditions are compared with the fault-free responses together with identical environmental inputs. This process is conducted using an evaluation of the change in the mean values and standard deviations of the loads and responses in the time domain as well as the spectra of the responses in the frequency domain. In addition, the effects of the faults on the floating offshore and onshore wind turbines are compared to distinguish the probable differences between them as well as

the severity of each fault for these two wind turbine types. To achieve the second objective, the structural responses under fault conditions for six 1-hr stochastic samples are compared with the fault-free responses to determine the change in the extreme values of the OWT and FWT responses.
The paper is organized as follows. Section 2 describes the theoretical background of the problem, including aeroelastic and hydrodynamic theories, controller configuration and fault simulation. Section 3 presents the load case set-up, the effects of faults on the performance parameters via a sensitivity analysis, the effect of faults on the extreme responses and a comparison between the effect of faults on the responses of OWT and FWT. Finally, Section 4 presents our conclusions.

### *1.1 Background*

Statistical data on wind turbine sub-system failure rates and downtime per failure are used to evaluate the reliability of wind turbines [18]. Reliability analyses of more than 6000 modern wind turbines and their sub-assemblies over 11 years in Denmark and Germany show that large wind turbines are less reliable than smaller ones due to increases in both the size of the wind turbines and the complexity of the wind turbine systems during this period. The average failure rate of pitch mechanisms for variable-speed pitch-regulated wind turbines is 0.4 per wind turbine per year and the mean time to repair for the pitch controller is approximately 70 hrs per failure. Ribrant and Bertling [19] showed that in Swedish wind power plants, 27.5% of the total failures in components between 2000-2004 were related to all sensors and pitch systems. In addition, 14.8% of the total downtime was due to sensors and blade/pitch systems. If the sensors and pitch mechanisms cannot be improved, fault diagnosis and fault tolerant control procedures are available to reduce the downtime. A recent study of detailed wind farm data, was conducted by Wilkinson et al. [20], who attempted to identify and understand the critical failures and their mechanisms in modern technology wind turbines. The results show that the pitch system is responsible for the largest contribution to both the failure rate and downtime of wind turbines at 15% and 20% respectively.
Prior to development of an efficient condition monitoring system, long-term experience was required as well as measurements during situations with faults and failures. Data measurement is costly and access to such a data is limited due to confidentiality of industrial projects. Because it is difficult, unsafe, expensive and potentially severely damaging to apply fault situations in full-scale wind turbines, simulation is the most useful approach to determining the relationship between the faults and several measurable parameters.

## 2. Theory

### *2.1 Environmental Loads*

Wind and wave loads are the two main environmental loads for offshore wind turbines. To perform a realistic load analysis for offshore structures, it is important to consider the correlation between the environmental loads. This effort requires a long-term joint probabilistic model of mean wind speed $U_m$ together with $H_s$ and $T_p$ [21]. If the wind speed is chosen as the primary parameter, the joint probability density function will be expressed as,

$$f_{U_m H_s T_p}(u,h,t) = f_{U_m}(u) f_{H_s|U_m}(h|u) f_{T_p|H_s U_m}(t|h,u) \quad (1)$$

The environmental data from the Statfjord site [21] (located at the crossing of the Norwegian and UK North Sea boundary) are used for this study. The Mann turbulence model is used to generate a full 3D turbulent wind field with correlation among the turbulence in the three directions. The hydrodynamic loads are induced by irregular waves. The Jonswap spectrum is used to simulate different sea states and each sea state is defined by an individual significant wave height $H_s$ and peak spectral period $T_p$.

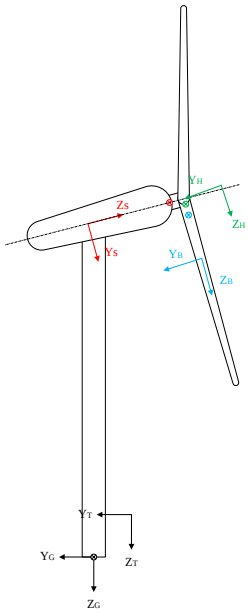


**Figure 1.** Orientation of the local coordinate systems on the main structural members in HAWC2 [15] (the origin of each coordinate system is shown by the ⊗ symbol and the same color) S: Shaft, B: Blade, H: Hub, T: Tower, G: Global

*2.2 Aeroelastic Model*

The aerodynamic loads on the wind turbine is based on the modified Blade Element Momentum (BEM) method [22] and the unsteady aerodynamic effects are modeled by Beddoes-Leishman type dynamic stall model [23]. The structural model in HAWC2 is based on a multi-body formulation with each body represented as a finite element model using a Timoshenko beam formulation. The structure consists of five sub structures: the tower, nacelle and rotor (three blades) for the onshore wind turbine and in addition the SPAR for the offshore floating wind turbine. The multi-body formulation allows for large rotations of the substructures. The orientations of the local coordinate systems are shown in Figure 1.

*2.3 Hydrodynamic Model*

The hydrodynamic loads on the spar floater in HAWC2 are calculated based on the Morison equation [24] and include the nonlinear hydrodynamic drag force. The wave kinematics (including regular and irregular airy waves) are calculated via the external DLL (Dynamic Link Library) and used within the HAWC2 code. The HAWC2 requires the hydrodynamic coefficients as inputs. The drag and inertia coefficients depend on the cross section of the SPAR and are given in offshore standards such as DNV-OS-J101 [25]. The nonlinear restoring forces from the mooring system are calculated from a quasi-static mooring-line module that accounts for the elastic stretching of an array of homogenous slack catenary lines. The natural periods for the three translational rigid body motions of the spar-type FWT in surge, sway and heave are 125 $sec$, 125 $sec$ and 31 $sec$, respectively and for the angular motions the roll, pitch and yaw natural periods are 30 $sec$, 30 $sec$ and 8 $sec$, respectively.

*2.4 Wind Turbine Controller*

The operational region from the cut-in wind speed to the cut-out wind speed is divided into below-rated and above-rated wind speed regions. In the below-rated wind speed region, the controller strategy captures the maximum power by maintaining a tip speed ratio close to $\lambda_{opt}$=6.36 and a pitch angle of $\beta_{opt} = 0\ deg$. At this region, the blade pitch controller is not activated, and the maximum power is achieved by adjusting the generator torque as a tabulated function of the filtered shaft speed. The low-pass filter is of first order with a time constant of 4 $sec$ to remove the free-free drive train vibration signal from the shaft speed measurement. In the above-rated wind speed region, the generator torque is constant and the controller attempts to maintain a constant shaft speed. The error between the filtered measured generator speed $\Omega_f$ and the rated generator speed $\Omega_{rat}$ is sent to the PI speed controller. The output of this PI controller is used as a reference pitch signal $\beta_{ref}$ for the pitch

system. Gain scheduling control of the pitch angle is implemented to compensate for the existing non-linear aerodynamic characteristics. The proportional ($KP$) and integral ($KI$) gains are defined as shown below,

$$KP(\beta) = KP_0.KG(\beta)\ , \qquad KI(\beta) = KI_0.KG(\beta), \qquad KG(\beta) = \frac{1}{1+\beta/KK} \tag{2}$$

where $KK = 6.3\ deg$ is the pitch angle at which the gain function is equal to 0.5 for the NREL 5-MW wind turbine. The pitch servo is modeled as a second-order system with a natural period of 2.1 $sec$ and a damping ratio of 0.9. To obtain a realistic response in the pitch angle control system, the servo mechanism model accounts for the min and max pitch angle limits of 0 $deg$ and 90 $deg$, respectively and a pitch rate limit of $\pm 8\ deg/sec$. The same controller as the FWT is used for the OWT with the following modifications. At above-rated wind speeds, a constant power strategy is used for the OWT instead of the constant torque used for the FWT. In addition, the constant proportional and integral ( $KP_0\ , KI_0$ ) gains of the FWT controller are increased to (0.019 , 0.008) compared with (0.006 , 0.001) [14].

A block diagram of the controller is illustrated in Figure 2. This figure shows how the faults are implemented in the controller loop. To simulate encoder faults, the fault model is placed in the path of the pitch sensor measurements. The pitch actuator faults are simulated by injecting a fault before the pitch actuator block. The mathematical models of the faults are shown in Table 1. The faults are initiated at a time $t = TTF$ (Time To Fault). To include the fault development time $T_t$, linear transition functions are defined from the fault-free ($t \leq TTF$) to fault condition, as listed in Table 1. The value of $T_t$ is selected such that the pitch rate after TTF remains below the maximum pitch rate ($\pm 8\ deg/sec$). Under the PASF, the pitch actuator command is $\beta_{act} = \beta_{dif}$ before the TTF. After the TTF, $\beta_{act}$ is shifted to the fault amplitude $\beta_{F0}$ with a linear slope of $(\beta_{F0} - \beta_{dif}(TTF))/(T_t)$. The slopes for the PSBF and PSFV are shown in Table 1.

When a fault occurs, an emergency shut-down might be initiated after fault detection. This is not considered in this paper and the main focus is on the steady-state response under the fault conditions. However the actual reason for the fault initiation is not understood and it is not clear that, how long exactly does it take for the fault to be developed, but to keep the stability in the numerical results it would be easier to make an incipient change from the fault-free state to the full-fault state. Therefore based on some physical constraint in the system, which is the max pitch rate of the pitch actuator, this transient state is defined. The sensitivity analysis has done to evaluate the effect of this transient part on the extreme response after the full-fault development. The results show that the extreme value in the response after the full fault development is independent from the time initiation of the fault and it is also larger than the extreme response in this transient period. But in the paper the whole time series is shown to illustrate how this fault development time is modeled. Due to high uncertainty in this transient part, this part of time series is not used for the statistical calculations.

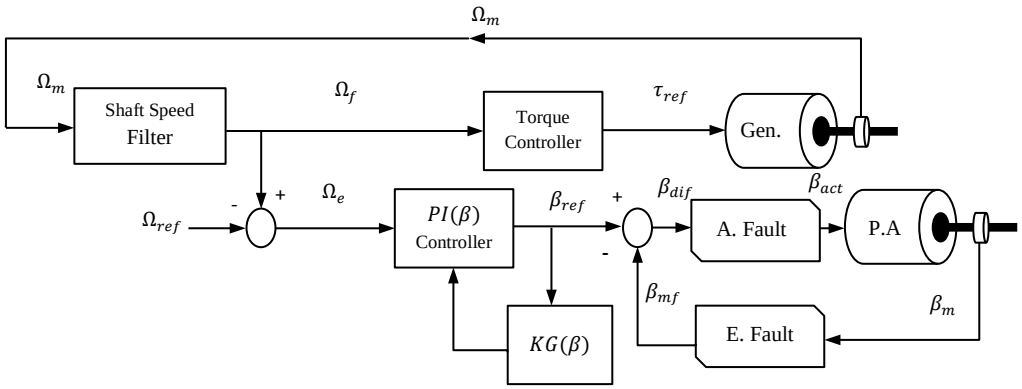


E : Encoder, P.A: Pitch Actuator, A: Actuator, Gen.: Generator, PI: PI Controller
$\Omega_m$: measured shaft speed, $\Omega_f$: filtered measured shaft speed, $\Omega_{ref}$: shaft speed reference, $\Omega_e$: shaft speed error,

**Figure 2.** Fault Implementation in HAWC2

**Table 1.** Mathematical Model of Faults

| Fault Type | $t \leq TTF$ | $TTF < t \leq TTF + T_t$ | $t > TTF + T_t$ |
|---|---|---|---|
| PASF | $\beta_{act} = \beta_{dif}$ | $\beta_{act} = (t - TTF)/T_t \cdot (\beta_{F0} - \beta_{dif}(TTF)) + \beta_{dif}(TTF)$ | $\beta_{act} = \beta_{F0}$ |
| PSBF | $\beta_{mf} = \beta_m$ | $\beta_{mf} = \beta_m(t) + (t - TTF)/T_t \cdot \beta_{F0}$ | $\beta_{mf} = \beta_m + \beta_{F0}$ |
| PSFV | $\beta_{mf} = \beta_m$ | $\beta_{mf} = (t - TTF)/T_t \cdot (\beta_{F0} - \beta_m(TTF)) + \beta_m(TTF)$ | $\beta_{mf} = \beta_{F0}$ |

TTF: Time To Fault, $\beta_m$: Measured blade pitch angle, $\beta_{mf}$: measured blade pitch angle by sensor under fault condition, $\beta_{F0}$: Fault amplitude, $\beta_{act}$: Actuator pitch angle, $\beta_{dif}$: Pitch angle difference, $T_t$: Fault development period

## 3. Simulation and Results

### *3.1 Load case setup*

In this study, the IEC 61400-3 design code [26] is used to define the load cases for the FWT. In particular, the "power production plus occurrence of controller system fault" is one of the design load cases in the IEC-61400-3 for offshore wind turbines. A range of wind speeds from 5 $m/s$ to 25 $m/s$ (cut-out) is divided into 11 equal bins with a bin size of 2 $m/s$. A wind turbine class CI with a reference turbulence intensity of $I_{ref} = 12\%$ and a reference wind speed of $V_{ref} = 50\ m/s$ is selected for this analysis. The turbulence intensity is calculated as a function of $U_m$ and the expected values of $H_s$ and $T_p$ are calculated for a given $U_m$ based on the joint distribution, as mentioned previously. The reference wind speed for the sea state distribution is the wind speed at 10 $m$ above the still water level, whereas the wind speed used for the wind turbine simulation is defined at the hub height. Therefore, the exponential shear profile with an exponent of 0.14 is used to estimate the wind speed at 10 $m$ above the still water level given the wind speed at the hub-height. For each fault case five different fault amplitudes ($\beta_{F0}$) are defined $\beta_{F0}$ =(0, 2, 5, 7, 11) $deg$, including zero fault amplitude for fault-free (Reference) load case. The total time length of each load case is 72 minutes (4300 $sec$). Data recording begins at $t = 400\ sec$ to remove the initial transient effect from the results. Thus 65 minutes (3900 $sec$) of simulation time are used for the analysis. The fault is initiated at $TFF = 200\ sec$. Investigation of the response under the fault condition with steady wind shows that the transient effect of the faults is always limited to the first 100 $sec$ after fault occurrence. Therefore, to remove the transient portion of the simulation after fault initiation, 100 $sec$ of the time series after $TFF$ is neglected and the remaining 1 $hr$ of the time series is considered as steady-state under fault conditions and is used for statistical analysis. The combination of 11 mean wind speeds and 5 fault amplitudes for each fault case results in 44 fault load cases and 11 fault-free load cases. To reduce the statistical uncertainties in the calculations, six realizations of each load case with six different seed numbers are simulated. The defined set of load cases and their wind speeds and fault amplitudes are listed in Table 2. These load cases are analyzed for each of the three fault cases (PASF, PSBF and PSFV) considered in this paper. The turbulence intensity, $H_s$ and $T_p$ for each $U_m$ are listed in Table 3.

**Table 2.** Set of load cases and relevant mean wind speeds and fault amplitudes for (time length=1 hr X 6 seeds)

| $\beta_{F0}$ [$deg$] \ $U_m$[m/s] | 5 | 7 | 9 | 11 | 13 | 15 | 17 | 19 | 21 | 23 | 25 |
|---|---|---|---|---|---|---|---|---|---|---|---|
| 0 | RC1 | RC2 | RC3 | RC4 | RC5 | RC6 | RC7 | RC8 | RC9 | RC10 | RC11 |
| F1=2 | LC1 | LC2 | LC3 | LC4 | LC5 | LC6 | LC7 | LC8 | LC9 | LC10 | LC11 |
| F2= 5 | LC12 | LC13 | LC14 | LC15 | LC16 | LC17 | LC18 | LC19 | LC20 | LC21 | LC22 |
| F3=7 | LC23 | LC24 | LC25 | LC26 | LC27 | LC28 | LC29 | LC30 | LC31 | LC32 | LC33 |
| F4=11 | LC34 | LC35 | LC36 | LC37 | LC38 | LC39 | LC40 | LC41 | LC42 | LC43 | LC44 |

**Table 3.** Sea state and turbulent intensity for each mean wind speed

| $U_m$[m/s] | 5 | 7 | 9 | 11 | 13 | 15 | 17 | 19 | 21 | 23 | 25 |
|---|---|---|---|---|---|---|---|---|---|---|---|
| $I$ [%] | 22 | 19 | 16 | 15 | 14 | 13 | 13 | 13 | 12 | 12 | 12 |
| $H_s$ [$m$] | 2.10 | 2.39 | 2.71 | 3.06 | 3.43 | 3.82 | 4.23 | 4.65 | 5.09 | 5.55 | 6.02 |
| $T_p$ [$sec$] | 9.55 | 9.62 | 9.74 | 9.89 | 10.05 | 10.24 | 10.43 | 10.63 | 10.85 | 11.06 | 11.24 |
| $\omega_p$ [$rad/sec$] | 0.658 | 0.653 | 0.645 | 0.635 | 0.625 | 0.614 | 0.602 | 0.591 | 0.579 | 0.568 | 0.559 |

In all the fault load cases, only the blade (2) is subjected to the faults. To illustrate the effect of each fault on the pitch sensor measurement of the blade (2), Figure 3 shows 400 *sec* of pitch sensor time series from LC17 compared with the fault-free response. The black dashed-line shows the fault-free response and the colored lines show the response under different fault conditions. The red line shows the effect of the PASF on the pitch sensor measurement. The blade pitch angle jumped to 5 *deg* at

TTF=200 $sec$. The green line shows the effect of the PSBF and the blue line shows the effect of the PSFV. The effects of the PASF and PSFV on the pitch angle sensor output are identical.
The pitch system controller is ideal at below-rated wind speeds; therefore, pitch sensor faults cannot affect the response at below-rated wind speeds. In the case of a pitch actuator fault, the fault can occur at above-rated wind speeds. When the rotor slows to below-rated wind speeds, faults can affect the response in this region.

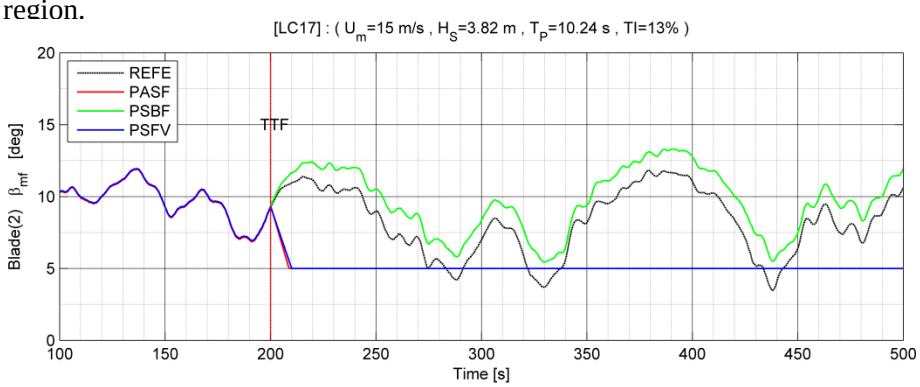


**Figure 3.** Pitch sensor time series of the blade (2) under different fault cases (LC17) compared with fault-free response (RC6) (**FWT**)
$T_P$: peak spectral period, $H_s$: significant wave height, $U_m$: mean wind speed, $\beta_{mf}$: blade pitch angle measurement under fault condition
$TTF$: Time to Fault

### *3.2 Sensitivity Analysis for the FWT*

To investigate the effects of the faults on the performance of the floating offshore wind turbine, the effects of each fault on the rotor speed, mechanical power, aerodynamic torque and thrust are studied as a function of the change in the mean value and standard deviation (SD) of each quantity. The shaft speed is one of the primary measurements for both the wind turbine controller and the safety system, and therefore, any change in the rotor shaft speed due to a fault can affect the response of the wind turbine. As an example, Figure 4 shows the effect of the PSFV on the mean and SD of shaft speed for all wind speeds and fault amplitudes. The PASF and PSBF had smaller effects on the shaft speed.

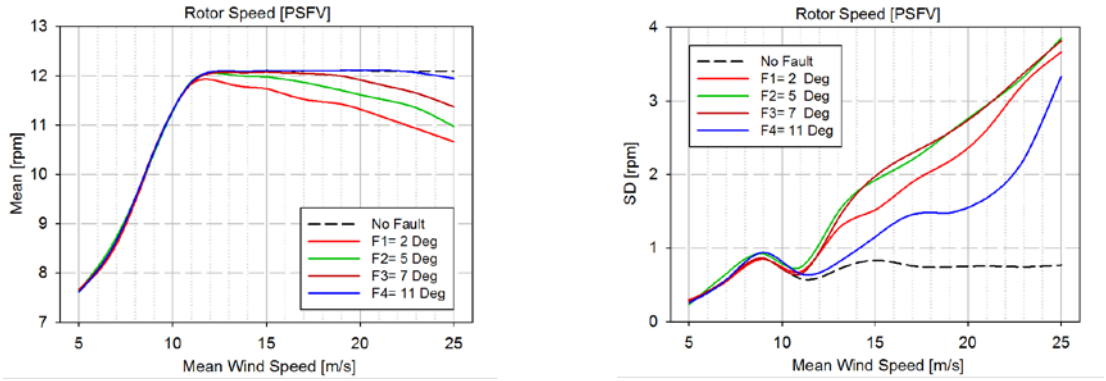


a) Mean Value of Rotor Speed b) Standard Deviation of Rotor Speed

**Figure 4.** Effect of pitch sensor fixed value (PSFV) on the rotor speed (F1-F4 : Fault amplitudes) (**FWT**)

At below-rated wind speeds, both the mean value and SD of the shaft speed were reduced due to the PASF. Under the PASF, the mean shaft speed was unchanged for high wind speeds. The rated rotor shaft speed (12.1 $rpm$) under the fault conditions was started at higher wind speeds than that of rated normal operation condition ($U_m > 11.4\ m/s$). The shaft speed SD was increased for all wind speeds at above-rated wind speed region. The PSFV and PSBF had different effects on the shaft speed. The mean value of the shaft speed was unchanged under the PSBF at the above-rated wind speeds, whereas it was reduced under the PSFV (Figure 4.a). The SD was increased under both the PSBF and PSFV and the PSFV had a much more severe effect (Figure 4.b).
The effects of the faults on the mean rotor power were almost the same as the effects of the faults on the rotor speed mean values. The mean value of the rotor mechanical power was reduced under the PASF at below-rated wind speeds and the rated power was shifted to the higher wind speeds. Until the rated power was reached, the pitch controller was not activated even though the wind speed was higher than the original rated wind speed. The SD of the power was only reduced at below-rated wind

speeds and the peak of the power SD was shifted to higher wind speeds under the PASF. The PSBF had rather limited effects on the mean value and SD of the power. The PSFV had much greater effect on the power SD than on the mean value. The main reason for this observation is that, with the increase in wind speed, the blade pitch angle was increased and the difference between the fault amplitude and actual blade pitch angle was also increased.

Figure 5 shows the effect of faults on the rotor aerodynamic thrust under the PSFV. The rotor thrust is important for tower vibration and global motion of the platform. At below-rated wind speeds, the PASF reduced the thrust and at above rated wind speeds, the peak of the thrust was shifted to higher wind speeds and the thrust was increased at wind speeds higher than 14 $m/s$. The PSBF had a minor effect on the thrust. The mean value and SD of the thrust were greatly increased by the PSFV (Figure 5), which can result in notably large structural responses.

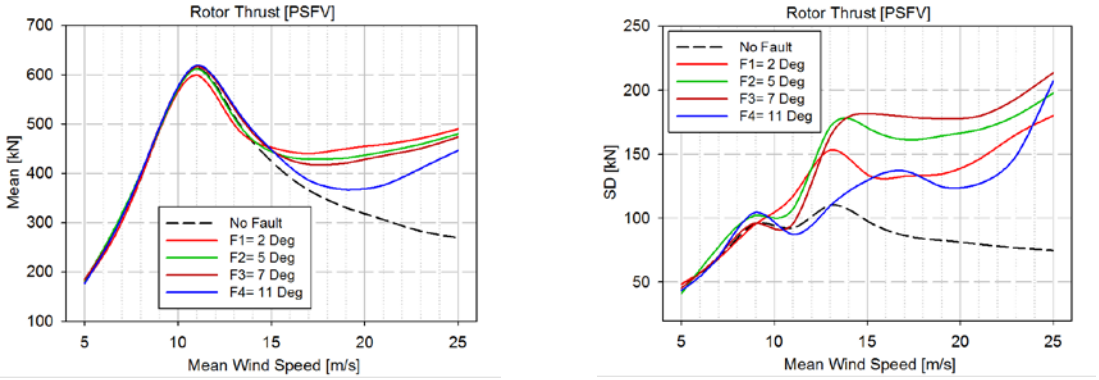


a) Mean value of rotor aerodynamic thrust b) Standard deviation of rotor aerodynamic thrust

**Figure 5.** Effect of the pitch sensor fixed value (PSFV) on the rotor aerodynamic thrust (F1-F4 : Fault amplitudes) (**FWT**)

To investigate how each fault case affects the performance parameters of the wind turbine, the effects of a fault in the blade (2) were evaluated on the other two blades. The collective blade pitch controller with individual pitch sensor measurements was used for this simulation. The pitch angle reference was calculated based only on the shaft speed error, which means that the sensor measurements of the blade (2) do not affect the two other blades directly. When a fault occurs in the blade (2), the aerodynamic torque is changed and consequently, the shaft speed is changed; therefore the controller will change the pitch angle set-point to adjust the shaft speed to the reference value (12.1 *rpm*). In Figure 6, the pitch angle time series of blades (1) and (2) are compared under all three fault cases for LC17. The mean wind speed for LC17 is 15 *m/s*. The blade pitch angle set point for this wind speed is 8 *deg*. The effects of the faults on the pitch angle of the blade (3) in all these fault cases were similar to those of the blade (1) and therefore only the results for the blade (1) are illustrated.

In the PASF (red line), the blade (2) moved to a 5 *deg* pitch angle at TTF=200 *sec*. The shaft speed was reduced and the controller changed the pitch angle of two other blades to maintain the constant shaft speed. The mean value of the pitch angle in blade (1) was increased to 9.5 *deg*, which was half of the change in the blade (2). This result means that, the sum of the changes in the blade (1) and (3) was equal to the total change in the blade (2) with the opposite sign, which could create a large unbalanced load on the shaft. The green lines show the effect of the PSBF. In this case, the blade (2) still followed the controller reference point with a -5 *deg* constant bias. Comparison of the blade (2) pitch angle from Figure 6 with the blade (2) pitch sensor measurements from Figure 3 shows that the pitch angle moved in the opposite direction of the pitch sensor measurement. The mean value of the pitch angle in this case was 5 *deg*. The effect of the PSBF on the blade (1) is similar to the effect of the PASF.

Under the PSFV, the system began to oscillate and exhibit a slow (30-50 sec) limit cycle. Under the fault condition, the mean pitch angle in the blade (2) was increased to 13 *deg* while the mean pitch angle of the blade (1) was reduced to 4.5 *deg*. Comparison of Figures 3 and 6 shows that, although a large oscillation occurred in the actual pitch angle of the blade (2), the pitch sensor displayed a constant value. The large SD in the responses under the PSFV is primarily due to this oscillation.

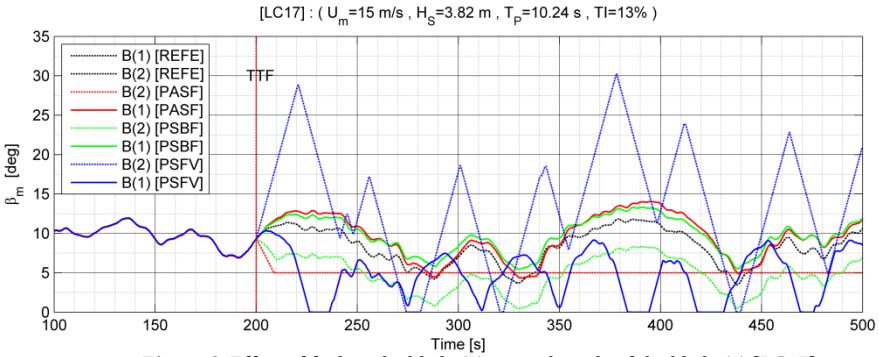


**Figure 6.** Effect of fault in the blade (2) on pitch angle of the blade (1) [LC17]
$T_P$: peak spectral period, $H_s$: significant wave height, $U_m$: mean wind speed,
$\beta_{mf}$: Blade pitch angle measurement under fault condition, $TTF$: Time to Fault

In fault-free operation conditions, there was no difference observed between the pitch angles of the three blades. Consequently, the bending moment on the shaft was primarily due to the tower shadow and gravitational load on the blades. Therefore, the mean values of the shaft bending moments were zero. Under the fault condition, a difference was observed between the pitch angle of the blade (2) and the two other blades, which cause a large change in the shaft bending moments. This difference generated a cyclic bending moment on the shaft and this bending moment on the shaft increased the torsional moment on the tower.

*3.3 Floater Response*

The rigid body motions of the FWT are excited by the wave loads on the floater, the rotor aerodynamic loads and the tower drag forces. The motions in surge and sway are limited by the catenary mooring line system, whereas the pitch and roll motions are ballast-stabilized. Changes in the thrust force directly affect the surge and pitch motions of the platform. The yaw motion of the spar is primarily excited by the bending moment on the shaft, which is transferred to the tower top through the shaft main bearing and gyroscopic moment due to coupling of the floater pitch motion and rotor angular motion. The results showed that yaw and pitch motions were highly affected by faults compared with four other DOFs.

The following figures present the effects of all faults on the spectra of the pitch and yaw motion responses for LC17. The pitch-resonant response was highly increased under the PSFV and the pitch spectra response showed two peaks. The first peak belongs to the pitch natural frequency at 0.2 $rad/s$ and the second peak denotes wave frequency response at 0.6 $rad/s$. Under fault conditions, the pitch frequency response was affected. The PSFV had a large effect on the surge and pitch motions compared to the two other faults. The pitch motion was more sensitive to faults compared with the surge motion.

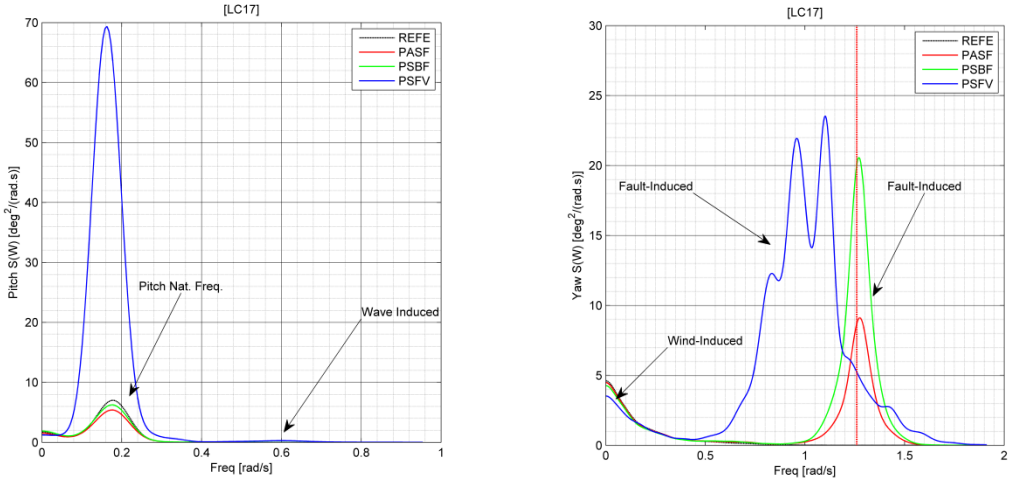


a) Pitch Spectra LC17 b) Yaw Spectra LC17

**Figure 7.** Effect of controller faults on pitch and yaw motions (6 hr steady-state, $U_m = 15\ \ m/s\,, H_s = 3.82\ m, T_P = 10.24\ s$)

The spar platform has a low yaw mooring stiffness. In addition, the moment of inertia around the tower Z-axis is small. Therefore, yaw motion can be excited by a small yaw moment. Due to the cylindrical shape of the floater, waves cannot induce platform yaw motion. The yaw moment on the platform was primarily due to the yaw misalignment, the imbalanced load on the rotor and gyroscopic effects. Under fault conditions, the bending moments on the shaft were increased, which led to a larger yaw moment. A comparison between the yaw motion peak frequency and shaft speed showed that the peak of the yaw response appeared at the rotor rotational speed (due to the 1P effect). For the PSBF and PASF, the bandwidth of the yaw response was narrower than the response under the PSFV. This effect originated from the large SD of the shaft speed and blade pitch angle under the PSFV.

### *3.4 Structural responses of the FWT*

This section presents the effect of faults on the extreme values as well as the mean and SD of the structural loads in the tower bottom (TB), shaft main bearing (SB), yaw bearing (YB) and blade root (BR). Six 1-hr stochastic samples were simulated for each load case to reduce the stochastic uncertainty in the calculations. To study the effect of the faults on the structural loads, certain reference values were calculated under normal operational conditions, as listed in Table 4. These reference loads include the short-term extreme value, the expected largest mean value and SD for each load component. The expected values of the loads under fault conditions were calculated (Table 5) and normalized by the corresponding values from normal operation (Table 4). The results are presented in Figures 8 and 9 as a ratio of fault load over normal load.

**Table 4.** Expected max loads on the selected structural components (FWT)

| Load Components | Expected Max Value | Largest Mean | Largest SD |
|---|---|---|---|
| Tower Bottom Mx $kNm$ | 152532 | 74296 | 29056 |
| Tower Bottom My $kNm$ | 54265 | 14766 | 10191 |
| Tower Bottom Mz $kNm$ | 13132 | 1232 | 2909 |
| Yaw Bearing Mx $kNm$ | 13226 | 2575 | 2654 |
| Yaw Bearing My $kNm$ | 10434 | 8451 | 1109 |
| Yaw Bearing Mz $kNm$ | 13101 | 1200 | 2910 |
| Shaft Mx $kNm$ | 3067 | 0 | 2758 |
| Shaft My $kNm$ | 2884 | 0 | 2766 |
| Shaft Mz $kNm$ | 5597 | 4180 | 549 |
| Blade Root Mx $kNm$ | 14861 | 8950 | 2685 |
| Blade Root My $kNm$ | 5932 | 998 | 2589 |

**Table 5.** Comparison of Fault and Fault-free Extreme response (FWT) (6 x 1hr samples)

| Load Components | Normal Operation | Parked | ETM | PAST | PSBF | PSFV |
|---|---|---|---|---|---|---|
| Tower Bottom Mx $kNm$ | 152532 | 301003 | 174457 | 177602 | 182423 | 291928 |
| Tower Bottom My $kNm$ | 54265 | 97714 | 72163 | 62788 | 65481 | 94136 |
| Tower Bottom Mz $kNm$ | 13132 | 8371 | 15720 | 30033 | 26944 | 45490 |
| Yaw Bearing Mx $kNm$ | 13226 | 8272 | 18048 | 30437 | 29352 | 69520 |
| Yaw Bearing My $kNm$ | 10534 | 23039 | 11139 | 11724 | 13006 | 20454 |
| Yaw Bearing Mz $kNm$ | 13101 | 2512 | 15703 | 30366 | 27173 | 45879 |
| Shaft Mx $kNm$ | 3067 | 14633 | 15256 | 18002 | 5292 | 38129 |
| Shaft My $kNm$ | 2884 | 6500 | 16297 | 37560 | 24580 | 53414 |
| Shaft Mz $kNm$ | 5597 | 23198 | 6168 | 5685 | 5508 | 7250 |
| Blade Root Mx $kNm$ | 14861 | 14177 | 18060 | 27243 | 16042 | 34157 |
| Blade Root My $kNm$ | 5932 | 11210 | 7992 | 11737 | 8910 | 18989 |

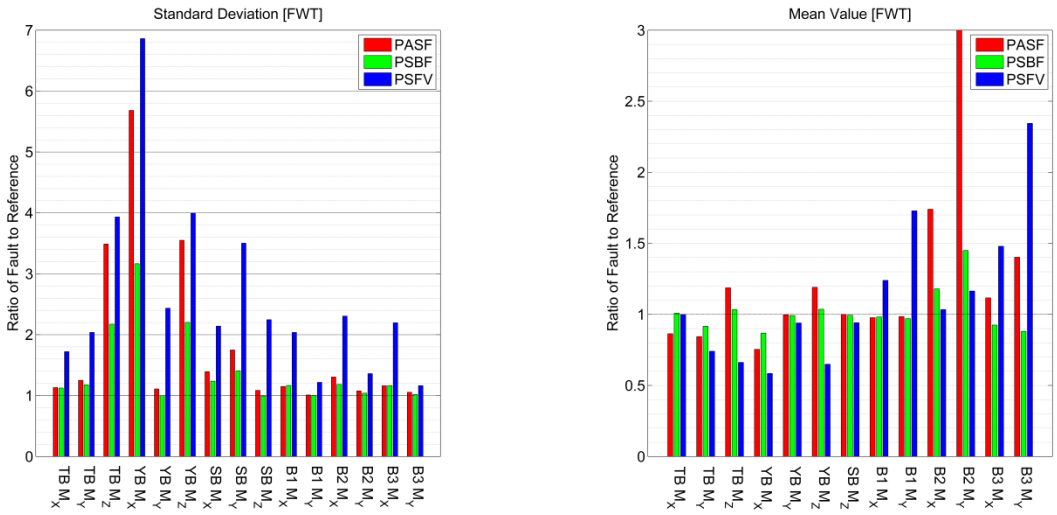


a) Standard Deviation b) Mean Value

**Figure 8.** Comparison of effect of faults on the Mean & SD (**FWT**)
(**TB**: Tower Bottom, **YB:** Yaw Bearing, **SB:** Shaft Bearing, **B1-B3**: Blade 1-3, **Mx:** Bending moment on X-axis, **My:** Bending moment on Y-axis, **Mz:** Torsional Moment on Z-axis) (6 x 1 hr samples)

The loads were calculated based on the local coordinate system of each component (see Figure 1). It is apparent from Figure 8(a) that the SD of the tower bending moments was not altered as much as the SD of the torsional moment and that the mean of tower fore-aft bending moment under the PASF was reduced. The latter was due to a reduction in the peak point of the mean aerodynamic thrust under the PASF. The relative changes in the mean shaft bending moments are not shown in the figures because the mean values were zero in the absence of faults. The PSFV had much larger effect on the vibrations (SD) compared with the two other fault cases, primarily due to the large oscillation in the blade pitch angle under this fault case.

Figure 9(a) shows the change in the extreme values for the FWT. The extreme values increased for all three fault cases. The major effect occurred on the shaft bending moment loads. In general, the effect of the PSFV was larger than that of the two other fault cases. The extreme values under the fault condition were always larger than that of the normal operational condition, primarily due to the imbalanced load on the rotor and the increase in the aerodynamic thrust force. For example, the extreme value of the tower bottom bending moment $M_x$ was increased by 14%, 18% and 89 % under the PASF, PSBF and PSFV, respectively.

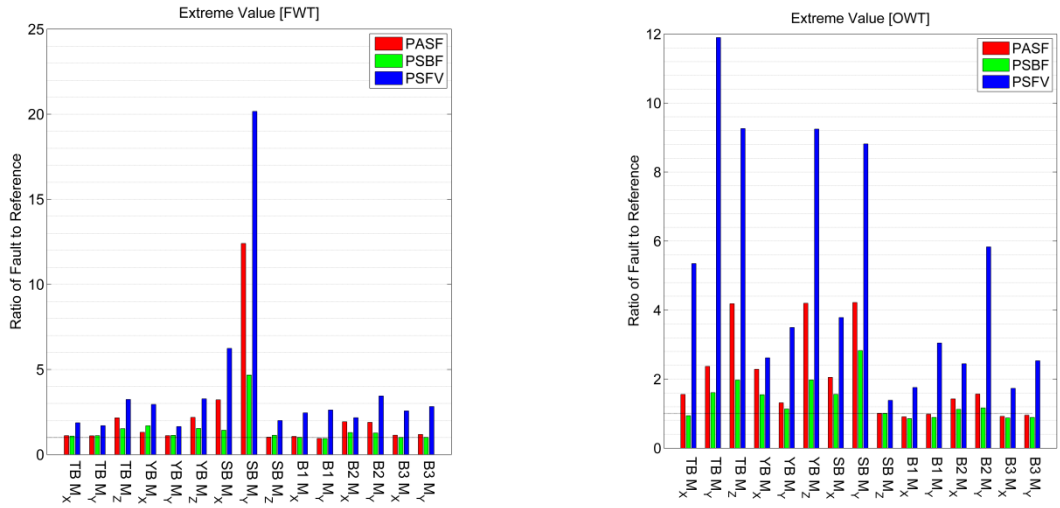


a) Floating Wind Turbine b) Onshore Wind Turbine

**Figure 9.** Comparison of effect of faults on extreme values for floating offshore and onshore wind turbines
(**TB**: Tower Bottom, **YB:** Yaw Bearing, **SB:** Shaft Bearing, **B1-B3**: Blade 1-3, **Mx:** Bending moment on X-axis, **My:** Bending moment on Y-axis, **Mz:** Torsional Moment on Z-axis) (6 x 1 hr samples)

The mean value of the yaw bearing bending moment around the Y-axis was nearly unchanged under fault conditions. The SD values of the yaw bearing fore-aft bending moment $M_x$ and the torsional moments $M_z$ were increased under fault conditions. The extreme values of the yaw bearing loads were all increased. The fore-aft bending moments and torsional moment were increased by greater than 300% and 200% under the PSFV, respectively. For yaw bearing, the main effect was on the SD and vibrations.

The mean values of the shaft bending moments were zero under normal operational conditions. Both the mean value and the SD of the shaft torque $M_z$ remained unchanged under the PASF and PSBF. The mean values of the shaft loads were more sensitive to faults than the SD. The extreme loads under fault conditions can be 3 to 20 times larger than under normal operational conditions.

The reference load characteristics on all three blades were almost equal. Under normal operational conditions, the flap-wise bending moment $M_x$ was the dominant load. The mean value of the loads on the blade (2), which was subjected to the fault, was increased under all fault conditions. The PSBF had a small effect on the mean value and the SD of two other blades. The extreme values of the blade loads were more sensitive to the PSFV compared with the other fault cases. As mentioned previously, only the blade (2) was subjected to the faults. Under the PASF and PSBF, the extreme loads on the blade (2) were larger than those of the two other blades and under the PSFV, the flap-wise bending moment on the blade (2) was smaller than on the two other blades.

To compare the extreme values under fault conditions with other potential extreme responses, two additional conditions from IEC were calculated. These extreme responses include operation under an extreme turbulent model (ETM) (DLC 1.3)[26] and the parked condition under extreme environmental conditions with a 50 years recurrence period. The extreme wind speed and sea state with a recurrence period of 50 years was calculated using the contour line method [27] for the selected offshore wind site. The extreme conditions based on the maximum mean wind speed and maximum significant wave height were calculated and listed in Table 6. For the parked conditions, two rotor azimuth positions were considered: blade (1) pointed upward and blade (1) pointed downwards.

**Table 6.** Environmental conditions on the 50-year contour surface

| Conditioned on | $U_{10m}$ | $H_s$ |
|---|---|---|
| $U_{hub}$ $[m/s]$ | 45 | 42.5 |
| $H_s$ $[m]$ | 13.5 | 15.3 |
| $T_P$ $[sec]$ | 15 | 15.5 |

Based on the results presented in Table 5, for the tower bending moment, the parked condition was the dominant load case. For the tower torsion, the PSFV was the dominant extreme load case. For the shaft bending moment as well as the blade bending moments, the extreme response under the fault cases was larger than those of other extreme load cases.

### *3.5 Comparison of the OWT and FWT under Fault Conditions*

In this section, the responses of an onshore wind turbine are compared with those of the floating offshore wind turbine under the same fault cases. The aim is to compare the effects of the faults on these two wind turbines. The reference extreme loads for the OWT were calculated with as similar methodology as for the FWT. To generate these results, a set of load cases similar to the FWT was used with certain modifications to the environmental conditions. The shear profile exponent and the reference turbulence intensity were increased from 0.14 to 0.2 and from 12% to 14%, respectively, according to the IEC 61400-1 [28]. The extreme responses under fault conditions for both wind turbines are compared in Table 7.

Comparison of the mean value and SD of the responses for the OWT and FWT under normal operation conditions shows that the blade loads were almost the same for both wind turbines. For the tower bottom and yaw bearing loads, except for the yaw bearing fore-aft bending moments, the loads in the FWT were larger than those of the OWT; the reason for this was the additional dynamic loads on the tower due to the motions of the floater in the FWT. The shaft loads in the FWT were smaller than those of the OWT, primarily due to the effect of the controller and constant torque strategy in the FWT controller.

**Table 7.** Comparison of Extreme Response (OWT and FWT) (6 x 1-hr samples)

| Load Components | FWT | | OWT | | |
|---|---|---|---|---|---|
| | Fault Case | Magnitude | Fault Case | Magnitude | RD |
| Tower Bottom Mx $kNm$ | PSFV | 291928 | PSFV | 561555 | 80 % |
| Tower Bottom My $kNm$ | PSFV | 94136 | PSFV | 825614 | 692 % |
| Tower Bottom Mz $kNm$ | PSFV | 45490 | PSFV | 80953 | 77 % |
| Yaw Bearing Mx $kNm$ | PSFV | 69520 | PSFV | 70680 | 1 % |
| Yaw Bearing My $kNm$ | PSFV | 20454 | PSFV | 24585 | 20 % |
| Yaw Bearing Mz $kNm$ | PSFV | 45879 | PSFV | 80142 | 74 % |
| Shaft Mx $kNm$ | PSFV | 38129 | PASF | 19144 | -49 % |
| Shaft My $kNm$ | PSFV | 53414 | PSFV | 67374 | 26 % |
| Shaft Mz $kNm$ | PSFV | 7250 | PSFV | 7889 | 8 % |
| Blade Root Mx $kNm$ | PSFV | 34157 | PSFV | 41752 | 22 % |
| Blade Root My $kNm$ | PSFV | 18989 | PSFV | 51260 | 169 % |

Figures 9(b)-10 show the change in the response characteristics of the OWT due to faults. The tower fore-aft bending moment and torsion in the FWT under the PASF and PSBF were larger than those of the OWT. The effect of the PSFV on the tower loads in the OWT was much larger than that of the FWT. The effect of faults on the yaw torsion of the OWT was larger than that of the FWT because the yaw stiffness of the OWT was larger than that of the FWT. The faults were more severe for the shaft loads in the FWT compared with the OWT. The extreme shaft loads under normal operation conditions in the OWT were larger than those of the FWT due to the constant power controller strategy at above-rated wind speeds and the larger turbulent intensity and shear profile slope for the OWT compared with the FWT. Under the fault condition, the increase in the shaft loads of the FWT was larger than those of the OWT. In the OWT, the PSBF and PASF had nearly the same effects on the blade loads, but the PSFV had a larger effect on the flap-wise bending moments of all three blades.

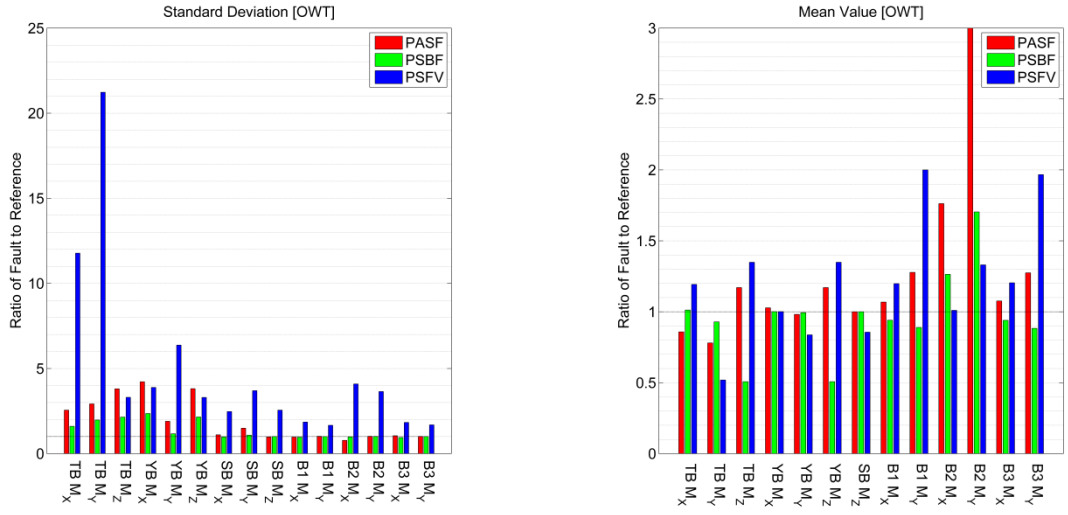


a) Standard Deviation b) Mean Value

**Figure 10.** Comparison of the effect of faults on the Mean & SD (**OWT**)(**TB**: Tower Bottom, **YB:** Yaw Bearing, **SB:** Shaft Bearing, **B1-B3**: Blade 1-3, **Mx:** Bending moment on X-axis, **My:** Bending moment on Y-axis, **Mz:** Torsional Moment on Z-axis) (6 x 1 hr samples)

## 4. Conclusions

The results presented in this work characterize the dynamic responses of the OC3-Hywind spar-type offshore floating wind turbine under blade pitch controller faults. Three fault cases in the blade pitch actuator and sensor were simulated and the effects of the faults were shown on the short-term extreme values in different structural members. The effects of the faults on the floater responses were also investigated. Finally, a comparison was conducted between the floating offshore and onshore wind turbines under fault conditions.

The results showed that different faults have fairly similar signatures. Sensitivity analysis showed that at below-rated wind speeds, the PASF reduced the responses because any change in the blade pitch angle reduced the torque on the rotor, which consequently reduced the power and aerodynamic

thrust. At above-rated wind speeds, the mean values were nearly unchanged due to the effect of the controller, whereas the extreme values and SD were increased. Under the PSFV, the responses were highly excited due to the slow limit cycle in the controller. The PSBF had a minor effect on the response compared to the other fault cases. The PSFV was found to be the most severe fault case for the floater response. The yaw motion was highly sensitive to all three fault cases due to the asymmetric loading on the rotor plane. The PASF and PSFV had limited effects on the other five DOFs of motions. Pitch and heave motions were also affected by the PSFV.

The effect of faults on the structural responses indicated that the shaft was the most risky component under fault conditions and the extreme loads under fault conditions might be 20 times larger than under normal operational conditions primarily due to imbalanced load on the rotor under the fault condition. The PSFV had the largest effect on all the structural responses. Under the PASF and PSBF, the extreme loads on the faulty blade were larger than those of the two other blades, whereas under the PSFV, the extreme loads on the faulty blade were smaller than the others.

Comparison of the extreme responses under fault conditions with other extreme responses showed that for the blade, shaft and yaw bearing, the extreme responses under the fault condition were dominant whereas for the tower, the parked condition was the dominant load case.

The comparison between the OWT and FWT under normal operation and fault conditions showed that, faults caused more damage in general to the tower and yaw bearing in the OWT, which is due to the dynamic characteristics (natural frequency) of the system and caused more damage to the shaft and blades of the FWT, which is due to the controller.

**Acknowledgement**

The authors gratefully acknowledge financial support from the Research Council of Norway granted through the Centre for Ships and Ocean Structures, NTNU. The authors also thank Erin E. Bachynski and Zhiyu Jiang for their useful discussions and comments.

## References

1. Larsen T. J. and Hanson T. D., *A method to avoid negative damped low frequent tower vibrations for a floating, pitch controlled wind turbine.* Journal of Physics: Conference Series, 2007. **75**(1): p. 012-073.
2. Wiggelinkhuizen E. J.; Braam H.; Rademakers L., V.T.W., *CONMOW: condition monitoring for offshore wind farms*, in *Wind Energy Report ECN-RX-03-036* (2003), Energy Research Centre, Netherlands.
3. Jiang Z., Karimirad M. and Moan T., *Steady State Response of a Parked Spar-type Wind Turbine Considering Blade Pitch Mechanism Fault*, in *International Offshore Polar Engineering Conference (ISOPE)*2012: Rhodes, Greece, June 17-22.
4. Cutululis N. A., Hansen A. D., Iov F. and S. P. *Grid Faults Impact on the Mechanical Loads of Active Stall Wind Turbine*. in *The Second International Symposium on Electrical and Electronics Engineering, ISEEE*. 2008. Galati, Romania, Aug 08-13.
5. Odgaard P. F.; Stoustrup J. and Kinnaert M., *Fault tolerant control of wind turbines: a benchmark model*, in *7th IFAC Symposium on Fault Detection, Supervision and Safety of Technical Processes* 2009: Barcelona, Spain, June 30 - July 3.
6. Odgaard P. F.; Stoustrup J.; Nielsen R. and Damgaard C., *Observer based detection of sensor faults in wind turbines*, in *European Wind Energy Conference* 2009: Marseille France, March 16-19.
7. Fang S., Leira B. J. and Blanke M., *Position mooring control based on a structural reliability criterion.* Structural Safety, 2013. **41**: p. 97-106.
8. Wei X., Verhaegen M. and Van Engelen T., *Sensor fault detection and isolation for wind turbines based on subspace identification and Kalman filter techniques.* International Journal of Adaptive Control and Signal Processing, 2010. **24**(8): p. 687-707.
9. Dalsgaard S., Blanke M. and Brath P., *Diagnosis of pitch and load defects*, May 2009, European Patents - EP 2225460-A2 B2.
10. Wei X. and Verhaegen M., *Sensor and actuator fault diagnosis for wind turbine systems by using robust observer and filter*. Wind Energy, 2011. **14**(4): p. 491-516.

11. Zaher A.; McArthur S. J., I.D.G., Patel Y.,, *Online wind turbine fault detection through automated SCADA data analysis.* J. of Wind Energy, 2009. **12**(6): p. 574-593.
12. Nielsen J. S.; Van de Pieterman R. P.; Sørensen J. D., *Analysis of pitch system data for condition monitoring.* Journal of Wind Energy, 2013, DOI 10.1002/we.1586.
13. Yang W.; Tavner P.J.; Crabtree C.J. and W. M., *Cost-effective condition monitoring for wind turbines.* Journal of Industrial Electronics, IEEE Transactions on, (2010). **57**(1): p. 263-271.
14. Jonkman J. M., B.S., Musial W., Scott G.,, *Definition of a 5-MW reference wind turbine for offshore system development*, 2009, National Renewable Energy Laboratory: Houston US.
15. Larsen T. J. and Hansen A. M., *How 2 HAWC2, the user's manual*, 2007, DTU Wind.
16. Jonkman J.M., *Definition of the Floating System for Phase IV of OC3*, 2010, National Renewable Energy Laboratory Huston US, Rep. No. NREL\TP-500-47535.
17. Blanke M., Kinnaert M., Lunze J. and Straroswiecki M., *(2006), Diagnosis and Fault-Tolerant Control, 2nd Edition, Springer*.
18. Tavner P. J.; Spinato F.; Bussel, G.J.W. and Koutoulakos E. *Reliability of different wind turbine concepts with relevance to offshore application*. in *European Wind Energy Conference (EWEC)*. 2008. Brussel, Belgium Mar.31-Apr.3: European Wind Energy Association.
19. Ribrant J. and Bertling L., *Survey of failures in wind power systems with focus on Swedish wind power plants during 1997-2005*, in *Power Engineering Society General Meeting, 2007. IEEE*2007, IEEE: Stockholm Denmark, Jun 24-28. p. 1-8.
20. Wilkinson M., H.B., Spinatz F., Gomez E., Bulacio H., Roca J., Tavner P., Feng Y., and Long H., *Methodology and results of the ReliaWind reliability field study*, in *European Wind Energy Conference (EWEC)*2010, European Wind Energy Association: Warsaw, Poland, April 20-23.
21. Johannessen K., Meling T. S. and Haver S., *Joint distribution for wind and waves in the northern north sea.* International Journal of Offshore and Polar Engineering, 2002. **12**(1).
22. Hansen M. O. L, *Aerodynamics of wind turbines* UK: Routledge, 2012.
23. Hansen, M.H., M. Gaunaa and H. Aagaard Madsen, *A Beddoes-Leishman type dynamic stall model in state-space and indicial formulations*2004.
24. Faltinsen O. M., *Sea loads on ships and offshore structures*. Ocean Technology, ed. Camberidge1990, UK: Cambridge university press.
25. DNV, *DNV-OS-J101 Offshore Standard, Design of Offshore Wind Turbine Structures*, 2004.
26. IEC, *IEC 61400-3*, in *Wind Turbines - Part 3: Design Requirements for Offshore Wind Turbines* 2009, International Electrotechnical Commission: Geneva, Switzerland.
27. Li L.; Gao Z. and Moan T. *Joint Environmental data at five european offshore sites for design of combined wind and wave energy devices*. in *32th International Conference on Ocean, Offshore and Arctic Engineering (OMAE 2013)* 2013, June 9-14. Nantes, France.
28. IEC 61400-1, *Wind turbines part 1: Design requirements*, in *International Electrotechnical Commission*2005, International Electrotechnical Committee: Geneva, Switzerland.